Magnetic origin of the chemical balance in alloyed Fe-Cr stainless steels: first-principles and Ising model study

E. Airiskallio[a], E. Nurmi[a], I. J. Väyrynen[a], K. Kokko[a,b,*], M. Ropo[c,1,2], M. P. J. Punkkinen[a], B. Johansson[d,e], L. Vitos[d,e,f]

[a] *Department of Physics and Astronomy, University of Turku, FI-20014 Turku, Finland*
[b] *Turku University Centre for Materials and Surfaces (MatSurf), Turku, Finland*
[c] *Department of Information Technology, Åbo Akademi, FI-20500 Turku, Finland*
[d] *Applied Materials Physics, Department of Materials Science and Engineering, Royal Institute of Technology, SE-10044 Stockholm, Sweden*
[e] *Department of Physics and Astronomy, Division of Materials Theory, Uppsala University, Box 516, SE-75120 Uppsala, Sweden*
[f] *Wigner Research Centre for Physics, Institute for Solid State Physics and Optics, H-1525 Budapest, PO Box 49, Hungary*

Abstract

Iron-chromium is the base material for most of the stainless steel grades. Recently, new insights into the origins of fundamental physical and chemical characteristics of Fe-Cr based alloys have been achieved. Some of the new results are quite unexpected and call for further investigations. The present study focuses on the magnetic contribution in the atomic driving forces related to the chemical composition in Fe-Cr when alloyed with Al, Ti, V, Mn, Co, Ni, and Mo. Using the *ab initio* exact muffin-tin orbitals method combined with an Ising-type spin model, we demonstrate that the magnetic

*Corresponding author. kalevi.kokko@utu.fi, tel. +358 2 333 5738
[1]Present address: Department of Physics, Tampere University of Technology, PL 692, FI-33101 Tampere, Finland
[2]COMP, Department of Applied Physics, Aalto University, P.O. Box 11100, FI-00076 AALTO, Finland

moment of the solute atoms with the induced changes in the magnetic moments of the host atoms form the main factor in determining the mixing energy and chemical potentials of low-Cr Fe-Cr based alloys. The results obtained in the present work are related to the designing and tuning of the microstructure and corrosion protection of low-Cr steels.
Keywords: First principles calculation, Ising model, Stainless steel, Corrosion protection, Fe, Cr, Al, Ti, V, Mn, Co, Ni, Mo, Magnetic moment, Mixing energy, Chemical potential

---

1. Introduction

The superb properties of stainless steel, like resistance to corrosion, high strength, good ductility, low maintenance and manufacturing cost, make it an ideal base material for a host of commercial applications. For example, stainless steels are used in cook-ware, cutlery, hardware, surgical instruments, major appliances, industrial equipment, automotive and aerospace structural alloy, and construction material in large buildings.

Stainless steel differs from corrodible carbon steel mainly by the amount of chromium in the bulk. Stainless steels have sufficient amount of chromium so that a thin and transparent film of chromium oxide rapidly forms on the open surface of the metal which prevents further surface corrosion and blocks corrosion from spreading into the internal structure of the material. More importantly, this oxide layer quickly reforms when the surface is scratched. This phenomenon is called 'self-healing passivation' and is seen also in other metals, such as aluminum and titanium.

High oxidation-resistance in air at ambient temperature is normally achieved

with chromium additions in steels. The observed steep increase of the corrosion resistance of the ferritic stainless steels starts when the Cr content in bulk reaches the level of about 10 at.% [1]. This bulk threshold of Cr in Fe-Cr random solid solutions correlates surprisingly well with the calculated reversal point of the sign of the difference between the effective chemical potentials in bulk and at the surface, $(\mu_{\mathrm{Fe}} - \mu_{\mathrm{Cr}})^{\mathrm{bulk}} - (\mu_{\mathrm{Fe}} - \mu_{\mathrm{Cr}})^{\mathrm{surface}}$. This reversal of the effective chemical potential is the cause for the segregation of Cr at the otherwise pure Fe surface of Fe-Cr alloys [2]. In addition to Cr, many other elements are frequently used as minor alloying components in stainless steels to further improve the properties of stainless steels grades. However their impact on the chemical potential of the host matrix is not well documented.

Alloying elements in steels can be divided into two main categories namely austenite and ferrite stabilizers. From the elements discussed in the present work Cr, Ti, Mo, V, and Al belong to the ferrite stabilizers and Ni, Mn, and Co are austenite stabilizers. In addition to the effect on the austenite/ferrite stabilization, these elements affect many other properties of steels. In the following we list some typical applications of alloying. Aluminum is often used in high temperature corrosion resistant materials [3–5] due to its ability to form a highly stable and protective oxide scale on the open surface when the material is exposed to oxidizing environment. The physical properties and corrosion resistance of Fe-Cr-Al as a function of the chemical composition of the alloy have been studied quite extensively [6–22]. Titanium is an element added to steels because it increases the strength and resistance to corrosion. Furthermore, Ti provides a desirable property to alloys: lightness.

Its density is less than half that of steel, so a titanium-steel alloy weighs less than ordinary steel and is more durable and stronger. These physical and mechanical properties make titanium steels an ideal material, for example, in aircraft and spacecraft engineering, chemical industry, and medicine [23–27]. Vanadium is a common component, for instance, in tool steels. Vanadium addition to Fe-Cr increases the hardness, tensile strength, wear resistance, and impact resistance [28, 29]. However, little has been published on the corrosion properties of the Fe-Cr-V alloys and on the role of vanadium in the passivation process [30–32]. Molybdenum is used to increase the strength to weight ratio and weldability [33].

Nickel is the most frequent alloying element to stabilize Fe-Cr alloys in the austenite structure. This crystal structure makes steels paramagnetic and less brittle at ambient conditions. Also manganese has been used in many stainless steel compositions. Manganese preserves the austenite structure in steels as does nickel, but at a lower cost. Austenite grades are perhaps the most widely used stainless steels in modern applications [23, 34]. Cobalt is used to increase heat and wear resistance (to improve anti-galling property) and to produce excellent magnetic properties and good ductility [35].

In this report, we investigate the role of minor alloying elements (Al, Ti, V, Mn, Co, Ni, Mo) on the balance of the chemical potentials of Fe and Cr and its consequences to surface properties. The basic data is obtained by an *ab initio* electronic structure method and in the subsequent analysis of the *ab initio* results we use an Ising-type spin model within a simple mean field approximation to elucidate the effects of magnetic interactions on the free energy of the alloy. The rest of the paper is divided into two main sections

and conclusions. The theoretical methods are briefly reviewed in Section 2 and the results are presented and discussed in Section 3.

2. Methods

The calculations are based on the density functional theory[36, 37] and performed using the Exact Muffin-Tin Orbitals (EMTO) method [38, 39]. The EMTO method is an improved screened Korringa-Kohn-Rostoker method [40], where the one-electron potential is represented by large overlapping muffin-tin potential spheres. By using overlapping spheres, one describes more accurately the crystal potential, when compared to the conventional non overlapping muffin-tin approach [41–43].

The EMTO basis set included s, p, d, and f orbitals. The one-electron equations were solved within the scalar-relativistic and soft-core approximation. The generalized gradient approximation in the PBE form was used for the exchange correlation functional [44]. The EMTO Green's function was calculated self-consistently for 32 complex energy points distributed exponentially on a semi-circular contour, which included states within 1 Ry below the Fermi level. In the one-center expansion of the full charge density, we adopted an l-cutoff of 8 and the total energy was calculated using the full charge-density technique [38, 42]. For each alloy the calculated equilibrium lattice constant was used. The convergence of the total energy with respect to the number of **k**-vectors was tested. It was found that 1240 uniformly distributed **k**-vectors within the irreducible wedge of the Brillouin zone was enough for the present purposes.

The Fe-rich Fe-Cr alloys adopt the body centered cubic (bcc) phase of

α-Fe. A number of previous works demonstrate that below the magnetic transition temperature (900-1050 K) the energetics of Fe-Cr alloys with less than 10% Cr is well described using the substitutionally disordered ferromagnetic bcc phase [45, 46].

Since in the present investigation we map a large concentration region with Cr content approaching zero, the conventional supercell method would require enormously large supercells. Here, we resolve this difficulty by employing the Coherent Potential Approximation (CPA) [47, 48]. Within the CPA, the alloy components are embedded in an effective medium, which is constructed in such a way that it represents, on the average, the scattering properties of the alloy. The EMTO approach in combination with the CPA has been applied successfully in the theoretical study of various structural and electronic properties of alloys and compounds [38] demonstrating the accuracy and efficiency needed for the present investigation.

The EMTO results are analyzed by using a spin model [49] where the magnetic moments obtained from the EMTO calculations are the input data and the output energy is used to calculate the effective chemical potential. This procedure allows a more transparent way to understand the effect of magnetism on the chemistry of the Fe-Cr-X alloys.

3. Results and discussion

3.1. Corrosion rate and chemical potentials

Our previous investigations demonstrate that the chemical composition of the close packed surfaces of Fe-Cr alloys, as a function of Cr content in bulk, follows closely the characteristic threshold-like behavior of the corro-

sion rate of ferritic stainless steels [2, 50]. In dilute, corrodible, $Fe_{1-x}Cr_x$ alloys ($x \lesssim 0.05$) the surfaces are predicted to be exclusively covered by Fe, whereas the Cr-containing surfaces become favorable when the bulk Cr concentration exceeds 10 at.%, which is close to the experimentally observed Cr threshold for corrosion resistant alloys. The discovered threshold point in the concentration of bulk Cr was found to be a consequence of the reversal of the relative magnitudes of the bulk and surface effective chemical potentials ($\mu_{\mathrm{Fe}} - \mu_{\mathrm{Cr}}$), which in turn reflects the peculiar electronic and magnetic structure of Fe-rich Fe-Cr alloys [45, 46, 49, 51–58].

In the present work we extend the previous investigations to research problems, such as to what extent the balance of the chemical potentials of Fe and Cr in bulk alloy can be tuned by doping Fe-Cr with minor alloying elements typically used in commercial steels. As a criterion for the alloying effect, we use the aforementioned threshold value of bulk Cr which corresponds to the breaking of the pure Fe surfaces. We calculate the effective chemical potential in bulk ($(\mu_{\mathrm{Fe}} - \mu_{\mathrm{Cr}})^{\mathrm{bulk}}$) for Fe-Cr-X alloys containing 5 at.% X (X=Al, Ti, V, Mn, Co, Ni, Mo) and compare the calculated $(\mu_{\mathrm{Fe}} - \mu_{\mathrm{Cr}})^{\mathrm{bulk}}$ (Fig. 1) to the corresponding effective chemical potential at the surface of binary Fe-Cr ($(\mu_{\mathrm{Fe}} - \mu_{\mathrm{Cr}})^{\mathrm{surface}}$), determined in our earlier work [2, 59, 60].

In alloys for which the surface energy of the third component X is higher than that of Fe, the surfaces are expected to be covered mainly by Fe atoms. Therefore, in these cases the effective chemical potential $\mu_{\mathrm{Fe}} - \mu_{\mathrm{Cr}}$ at the surface can be approximated by that of the binary Fe-Cr alloy and in these alloys the threshold value of bulk Cr corresponds to the onset of the breaking of the pure Fe surface by Cr atoms. On the other hand, for those alloys where

the surface energy of the third component X is lower than that of Fe (Al and Ni) [61]), the surfaces of the Fe-Cr-X alloys are expected to be covered mainly by X atoms. In these cases the lowering of the threshold value of bulk Cr corresponds to the increasing of the driving force for moving an Fe atom, compared to that of Cr, from the surfaces to the bulk of the alloy.

By comparing the effective chemical potential $\mu_{\rm Fe} - \mu_{\rm Cr}$ in bulk and at the surface we are able to estimate, for ternary Fe-Cr-X alloys, the threshold concentrations of bulk Cr, which in turn are expected to be related to the onset of the high corrosion resistance in Fe-Cr based alloys. The first-principles EMTO results for the threshold values ($c_{\rm thr}$) of bulk Cr in $\mathrm{Fe}_{1-x-0.05}\mathrm{Cr}_x\mathrm{X}_{0.05}$ alloys are listed in Table 1. Compared to the undoped Fe-Cr the dopants, with the exception of Mn, shift the threshold value down. In fact, as Fig. 1 shows, these dopants shift down the effective chemical potential within the whole investigated concentration range $0 \lesssim c_{\rm Cr}^{\rm bulk} \lesssim 20$ at. %. Therefore, if the driving force for the surface would come exclusively from the bulk, then Cr content at the surface would increase accordingly. This effect can be estimated by solving the differential equation for internal energy and entropy ($dU = TdS$), in a similar way as was done in our previous investigation [51]. For the surface concentration of the undoped $\mathrm{Fe}_{0.9}\mathrm{Cr}_{0.1}$ at 300 K we obtain 16 at. % Cr at the surface. When 5 at. % of Fe is replaced with the doping elements the Cr content at the surface is increased to about 25 at. % for Al, Co, and Mo, 30 at. % for V, and 35 at. % for Ni and Ti dopants. Doping with Mn reduces the surface concentration of Cr to about 5 at. %. However, in the case of Al and Ni dopants the surface is expected to be covered mainly by these dopant atoms due to their lower surface energy.

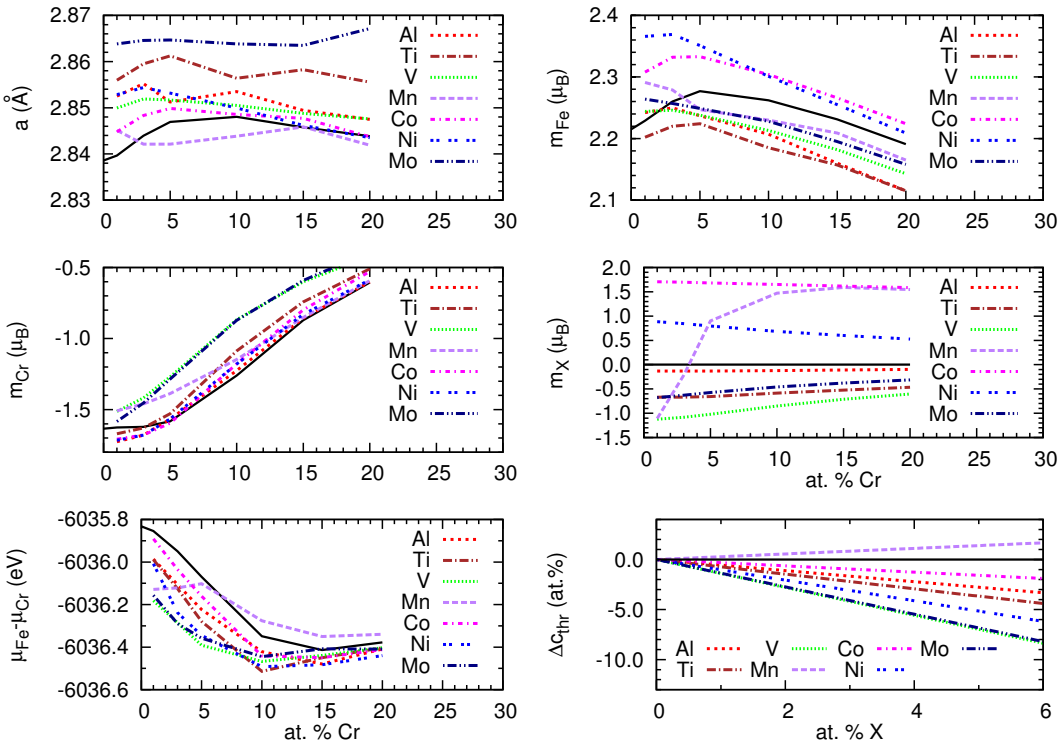

Figure 1: (Color online) Results of the EMTO calculations. Lattice parameter (a), magnetic moment per atom (m, in Bohr magnetons μ_{B}), effective chemical potential in bulk ($\mu_{\mathrm{Fe}} - \mu_{\mathrm{Cr}}$) and the shift of the Cr threshold Δc_{thr} of $\mathrm{Fe}_{1-x-0.05}\mathrm{Cr}_x\mathrm{X}_{0.05}$ where X is the alloying component (Al, Ti, V, Mn, Co, Ni, Mo). Continuous black curve shows the results for binary Fe-Cr. Δc_{thr} as a function of X content is a linear approximation based on 5 at.% X data.

X	Al	Ti	V	Mn	Co	Ni	Mo	Cr
c_{thr} (at.%)	5	4	1	9	6	3	1	8

Table 1: Results, based on our *ab initio* calculations, for the threshold values of bulk Cr corresponding to the reversal of the directions of the Cr and Fe driving forces towards the surface in $Fe_{1-x-0.05}Cr_xX_{0.05}$ alloys. The data is obtained by determining the intersection point of the calculated $(\mu_{\mathrm{Fe}} - \mu_{\mathrm{Cr}})^{\mathrm{bulk}}$(Fig. 1) and $(\mu_{\mathrm{Fe}} - \mu_{\mathrm{Cr}})^{\mathrm{surface}}$ [2]. The last column (Cr) shows the threshold value for binary Fe-Cr alloys, which agrees well with the experimentally observed onset point of corrosion protection in Fe-Cr, $\sim$ 10 at. % Cr in bulk [1]. All investigated alloying elements, except Mn, are expected to improve the corrosion resistance at lower Cr contents compared to the binary Fe-Cr alloy.

3.2. Chromium threshold versus volume of the Fe-Cr based alloys

Plotting the data shown in Table 1 as a function of the lattice parameter (a) of the alloy (Fig. 2) reveals an overall decreasing trend of the Cr threshold value with the volume of the alloy. The obtained general trend shown in the relation between the Cr threshold value and the volume of the alloy can be understood by considering the total energy of the alloy. The inversely proportional relation between the Cr threshold value c_{thr} and the lattice parameter of the alloy a can be elucidated as follows:

(i) The increased volume is related to the decreased bonding between the atoms, and consequently to the increased total energy of the alloy.

(ii) The increasing total energy of dilute Fe-Cr alloys decreases the magnitude of the negative slope of the mixing enthalpy of $Fe_{1-x}Cr_x$ at $x \approx 0$. This is due to the characteristic shape of the mixing enthalpy of $Fe_{1-x}Cr_x$ alloys at small x as seen in *ab initio* results [2] and also in

spin model calculations (Fig. 3)

(*iii*) The relation between the effective chemical potential of bulk Fe-Cr and the slope of the mixing enthalpy (ΔH) of the alloy [62]

$$(\mu_{\mathrm{Fe}} - \mu_{\mathrm{Cr}})^{\mathrm{bulk}} \approx -\frac{\partial \Delta H}{\partial x} + \text{constant} \tag{1}$$

shows that the effective chemical potential at $x \approx 0$ consequently decreases.

(*iv*) Finally, the decrease of $(\mu_{\mathrm{Fe}} - \mu_{\mathrm{Cr}})^{\mathrm{bulk}}$ at small x shifts the threshold value c_{thr} for the Cr burst to the surface to lower Cr contents.

One should note that there is also a coarse correlation between the initial slope of the lattice parameter a versus chromium content x and the shift of the Cr threshold Δc_{thr} as depicted in Fig. 1. At this point it is clear that vanadium deviates significantly from the overall trend of c_{thr} with volume showing the largest reduction in the bulk Cr threshold with increasing volume (Fig. 2). Therefore, besides on the volume, the threshold value of the bulk Cr depends also on other parameters, an issue that we will investigate in the next section.

3.3. Role of magnetic interactions in the thermodynamics of Fe-Cr and its derivatives

Because the phase stability of Fe-Cr alloys depends significantly on the magnetic interactions between the constituent atoms [2, 49–51, 63, 64], it is also instructive to concentrate on the magnetic properties when searching the physical parameters that determine the Cr threshold in Fe-Cr alloys. In

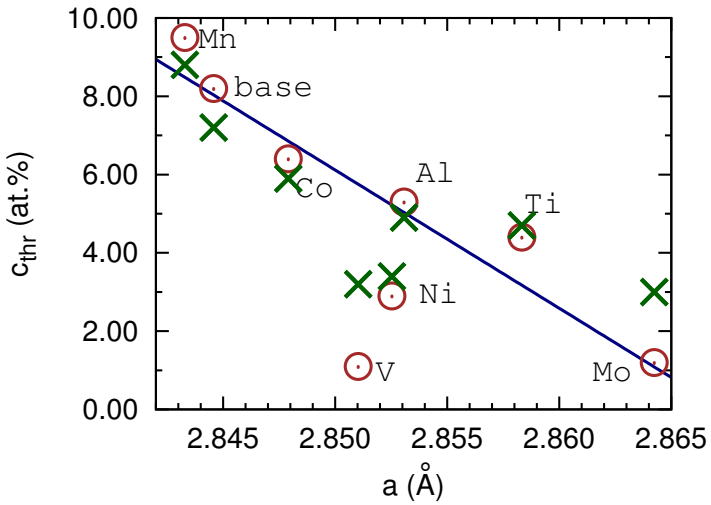

Figure 2: (Color online) Threshold of the Cr concentration in ternary $Fe_{1-x-0.05}Cr_xX_{0.05}$ alloys (X = Al, Ti, V, Mn, Co, Ni, Mo; base refers to binary Fe-Cr) as a function of the lattice parameter a. The brown circles show the EMTO results and the green crosses show the spin-model results. The straight line is a guide for an eye showing the general trend with the lattice parameter.

order to trace the role of the additional alloying elements (X) on the magnetic contribution to the bulk threshold of Cr in Fe-Cr-X alloys we analyze our *ab initio* results by using a spin Hamiltonian

$$H_{ij} = (S_i + S_j)\sigma_i\sigma_j/2 + (1 - S_iS_j)\sigma_i\sigma_j/2. \tag{2}$$

A similar Hamiltonian was employed by Ackland [49] in his study of the Fe-Cr systems. The total energy of the N atom system ($E_{\rm tot}$) per atom then reads

$$E_{\rm tot}/{\rm atom} = \frac{1}{N}\sum_{i=1}^{N}\frac{1}{2}\sum_{j=1}^{14}H_{ij} = \frac{1}{N}\sum_{i=1}^{N}H_i =< H_i >, \tag{3}$$

where the j summation runs over the nearest and next nearest neighbors of the site i (14 sites in the bcc lattice [49]). Applying equation (3) to binary

Fe-Cr alloy, we adopt $S_{\rm Fe} = -1$, $S_{\rm Cr} = 1$, and $\sigma_{\rm Fe}$ and $\sigma_{\rm Cr}$ are the magnetic moments of Fe and Cr atoms, respectively. This yields ferromagnetic Fe-Fe coupling and antiferromagnetic coupling of Cr to its neighbors. Within the CPA formalism, we obtain for the $Fe_{1-x}Cr_x$ alloy

$$\begin{aligned} < H_i > &= x < H_{\rm Cr} > +(1-x) < H_{\rm Fe} > \\ &= 7(x^2\sigma_{\rm Cr}^2 + 2x(1-x)\sigma_{\rm Cr}\sigma_{\rm Fe} \\ &- (1-x)^2\sigma_{\rm Fe}^2). \end{aligned} \quad (4)$$

Since we are interested in the relative energy balance of Cr in bulk, we extend the above spin model to Fe-Cr-X by merging the X atoms with the Fe atoms to form an effective Fe matrix into which Cr atoms are dissolved. For individual spins σ we use the calculated magnetic moments (Fig. 1). The spin of the effective Fe matrix is taken to be the average of the magnetic moments of the Fe and X atoms weighted by their concentrations. As Fig. 3 shows, the alloying of Fe-Cr changes both the curvature and the position of the minimum of the total energy (mixing enthalpy), particularly around the point of 5 at.% Cr which is an important region with respect to the bulk Cr threshold. Because the bulk effective chemical potential $(\mu_{\rm Fe} - \mu_{\rm Cr})^{\rm bulk}$ is a key quantity in determining the bulk Cr threshold and since the effective potential is practically the derivative of the total energy (Eqn. (1)) we calculate the derivatives of the spin model total energies from Fig. 3. The result is shown in Fig. 4. The derivatives of the total energy of the spin model have approximately the same shape as the *ab initio* EMTO effective chemical potentials $(\mu_{\rm Fe} - \mu_{\rm Cr})^{\rm bulk}$, shown in Fig. 1. Plotting in Fig. 4 the surface chemical potential $(\mu_{\rm Fe} - \mu_{\rm Cr})^{\rm surface}$ of Fe-Cr alloy, we can estimate

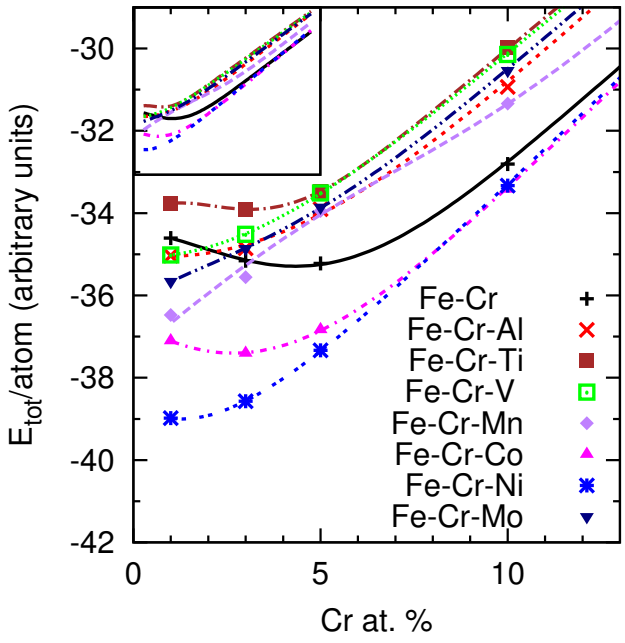

Figure 3: (Color online) The total energy per atom obtained from the spin model. The symbols refer to the results of the spin model (Eqn. (4)) and curves are functions fitted to the spin model data. The inset shows the same results but from 1 to 20 at.% Cr emphasizing the almost linear behavior of the energy as obtained from the spin model within the 10–20 at.% Cr range.

the bulk Cr thresholds $c_{\rm thr}$ by determining the positions of the intersections of the $(\mu_{\rm Fe} - \mu_{\rm Cr})^{\rm bulk}$ and $(\mu_{\rm Fe} - \mu_{\rm Cr})^{\rm surface}$ curves. These estimated critical compositions are shown by green crosses in Fig. 2. The spin model based Cr threshold deviates clearly from that of the EMTO calculations in the case of V and Mo. But what is important here, is that the general trend predicted by the spin model agrees well with the EMTO result. This suggests that the spin model is capable of capturing the main features of the Fe-Cr-X alloy and to reveal the underlying magnetic interactions. The obtained shifts of

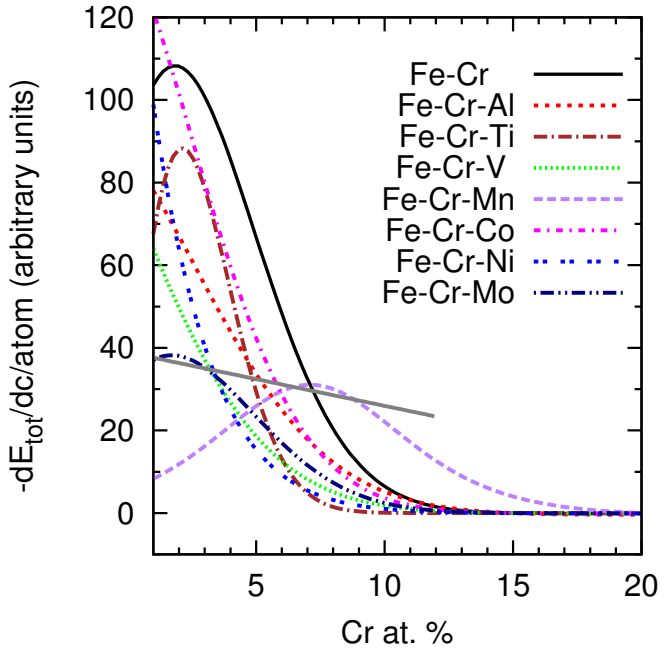

Figure 4: (Color online) The derivative of the spin model total energy per atom (spin model, Fig. 3) multiplied by -1 and shifted to the common zero value at Cr at.% = 20. The short gray line segment shows the level of the EMTO surface effective chemical potential $((\mu_{\rm Fe} - \mu_{\rm Cr})^{\rm surface}$ [2] relative to the Fe-Cr curve.

the thresholds of bulk Cr ($\Delta c_{\rm thr}$) due to the alloying in the spin model agree surprisingly well with those obtained directly from the EMTO calculation (Fig. 5). Presenting the results using the relative quantities,

$$\frac{\Delta c_{\rm thr}}{c_{\rm thr}({\rm Fe-Cr})} = \frac{c_{\rm thr}({\rm Fe-Cr-X}) - c_{\rm thr}({\rm Fe-Cr})}{c_{\rm thr}({\rm Fe-Cr})} \qquad (5)$$

shown in Fig. 6, it is realized that there is a significant correlation between the relative thresholds obtained from the EMTO calculation and the spin model estimates demonstrating that the effective chemical potential of Fe and Cr in the investigated alloys is to a large extent determined by magnetic interactions. This conclusion supports investigations that suggest the

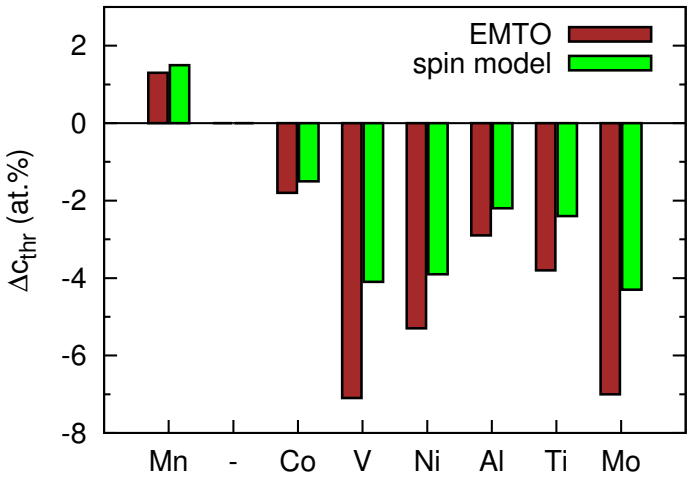

Figure 5: (Color online) The shifts of the bulk Cr threshold $\Delta c_{\rm thr}$ from that of the Fe-Cr case (for Fe-Cr: EMTO $c_{\rm thr} = 8$ at.%, spin model $c_{\rm thr} = 7$ at.%) due to 5 % alloying with Al, Ti, V, Mn, Co, Ni, and Mo, obtained by the EMTO method (brown bars) and the spin model (green bars). Except for Mn, the spin model predicts smaller shifts.

corrosion protection of Fe-Cr alloys to be to some extent of magnetic origin.

We close our discussion by analyzing the EMTO results shown in Fig. 1. The general trend seen in Fig. 1 is that all investigated alloying components lower the $(\mu_{\rm Fe} - \mu_{\rm Cr})^{\rm bulk}$ for low-Cr alloys. When Cr content increases, this trend is diminished or reversed (Mn). When Cr content reaches 15–20 at.% the effect of the additional alloying is small. Manganese shows the most peculiar behavior: below 5 at.% Cr, Mn strongly decreases $(\mu_{\rm Fe} - \mu_{\rm Cr})^{\rm bulk}$ whereas above 10 at.% Cr it increases $(\mu_{\rm Fe} - \mu_{\rm Cr})^{\rm bulk}$.

Maybe the most interesting data in Fig. 1 is related to the magnetic moments of Mn. It provides an illustrative evidence for the decisive role of the magnetic moments of the alloying elements in the relative balance between the bulk chemical potentials of Fe and Cr in Fe-Cr-X alloys. While Cr con-

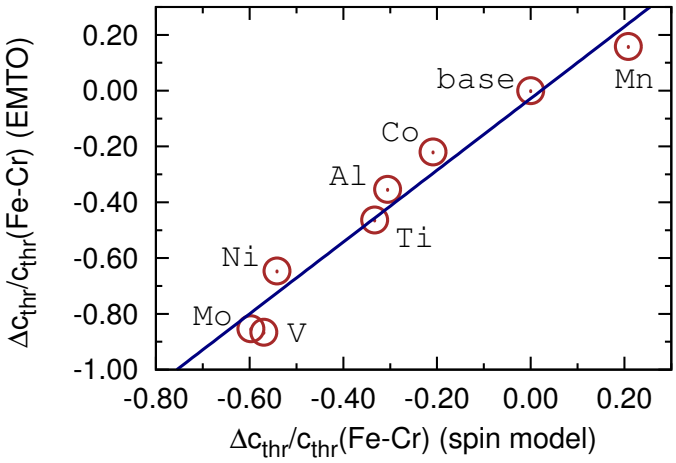

Figure 6: (Color online) Relative shift of the threshold of the Cr concentration $\Delta c_{\rm thr}/c_{\rm thr}({\rm Fe-Cr})$ in $Fe_{1-x-0.05}Cr_xX_{0.05}$ with (X = Al, Ti, V, Mn, Co, Ni, and Mo; base refers to Fe-Cr). The line shows the linear fit to the data $f(x) = a + bx$, $a = -0.028$ $b = 1.29$.

centration changes from 0 to 5 at.% the Mn moment changes approximately from -1 to $+1$ Bohr magneton ($\mu_{\rm B}$) i.e. practically through the whole range of the moments of the investigated additional alloying elements (from V to Co). Correspondingly the $(\mu_{\rm Fe}-\mu_{\rm Cr})^{\rm bulk}$ changes from the value of the Fe-Cr-V case to that of the Fe-Cr-Co case revealing the crucial role of the magnetic moment of the alloying element on the chemical potentials in Fe-Cr alloys.

4. Conclusions

Using density functional theory, implemented in the *ab initio* EMTO formalism, and a spin model, we investigated the effective chemical potential $(\mu_{\rm Fe}-\mu_{\rm Cr})^{\rm bulk}$ and showed that the magnetic moment of the doping atom (X = Al,Ti,V,Mn,Co,Ni,Mo) plays a significant role in the energy balance of Fe and

Cr atoms in Fe-Cr-X alloys. The employed combined computational method provides an efficient tool to scan the effects of different alloying components at any concentration. Since the stainless property of Fe-Cr based alloys is related to the presence of Cr near the alloy surface, i.e. related to $(\mu_{\mathrm{Fe}} - \mu_{\mathrm{Cr}})^{\mathrm{bulk}}$, our investigation provides new data in understanding and tuning the corrosion resistance of the Fe-rich Fe-Cr based alloys. Using the obtained results for the bulk it is possible to estimate the magnetic enhancement of the driving force of Cr from the bulk to the surface due to a third component of the alloy.

5. Acknowledgements

The computer resources of the Finnish IT Center for Science (CSC) and Mgrid project are acknowledged. Financial support from the Academy of Finland (Grant No. 116317) (EA, EN, KK) and Outokumpu Foundation (EA) are acknowledged. The Swedish Research Council, the European Research Council, the Swedish Steel Producer's Association (LV, BJ), the Hungarian Research Fund (OTKA projects 84078 and 109570) (LV) and the Göran Gustafson Foundation (MP) are also acknowledged.

[1] G. Wranglén, An Introduction to Corrosion and Protection of Metals, Chapman and Hall, New York, 1985.

[2] M. Ropo, K. Kokko, M.P.J. Punkkinen, S. Hogmark, J. Kollár, B. Johansson, L. Vitos, Phys.Rev. B 76 (2007) 220401(R).

[3] S.L. Case, K.R. van Horn in: Aluminum in Iron and Steel, Alloys of

Iron Research Monograph Series ed. F.T. Sisco, John Wiley and Sons, Inc., New York, 1953.

[4] A.S. Khanna, Introduction to High Temperature Oxidation and Corrosion, Materials Park, OH, AMS International, 2002.

[5] A.S. Khanna, High temperature oxidation, Handbook of Environmental Degradation of Materials, ed. M. Kutz, William Andrew Publishing, Norwich, NY, 2005 pp.105–152.

[6] Y. Niu, S. Wang, F. Gao, Z.G. Zhang, F. Gesmundo, Corrosion Science, 50 (2008) 345.

[7] P. Tomaszewicz, G.R. Wallwork, Rev. High Temp. Mater. 4 (1978) 75.

[8] B.A. Gordon, W. Worrell, V. Nagarajan, Oxidation of Metals 13 (1979) 13.

[9] G.B. Abderrazik, G. Moulin, A.M. Huntz, E.W.A. Young, J.H.W. de Wit, Solid State Ionics 22 (1987) 285.

[10] F.H. Stott, Rep. Prog. Phys., 50 (1987) 861.

[11] F.H. Stott, F.I. Wei, Oxidation of Metals 31 (1989) 369.

[12] R. Prescott, M.J. Graham, Oxidation of Metals 38 (1992) 73.

[13] J.H. DeVan, P.F. Tortorelli, Corrosion Science 35 (1993) 1065.

[14] I. Gurrappa, S. Weinbruch, D. Naumenko, W.J. Quadakkers, Materials and Corrosion 51 (2000) 224.

[15] C. Schwalm, M. Schütze, Materials and Corrosion 51 (2000) 161.

[16] N. Babu, R. Balasubramaniam, A. Ghosh, Corrosion Science 43 (2001) 2239.

[17] D.B. Lee, G.Y. Kim, J.G. Kim, Materials Science and Engineering A339 (2003) 109.

[18] I.G. Wright, R. Peraldi, B.A. Pint, Mater. Sci. Forum 461–464 (2004) 579.

[19] J.A. Nychka, D.R. Clarke, Oxidation of Metals 63 (2005) 325.

[20] V. Rohr, Development of novel protective high temperature coatings on heat exchanger steels and their corrosion resistance in simulated coal firing environment, PhD dissertation, Centre Interuniversitaire de Recherche et d'Ingénierie des Matériaux (CIRIMAT) (2005).

[21] H.J. Grabke, Materiali in Tehnologije 40 (2006) 39.

[22] H. Asteman, M. Spiegel, Corrosion Science 50 (2008) 1734.

[23] D. Cismaru, Corrosion Science 5 (1964) 47.

[24] M.J. Bennet, M.R. Houlton, Journal of Nuclear Materials 87 (1979) 81.

[25] A. Freiburg, W. Jäger, J. Flügge, Fresenius J. Anal. Chem. 341 (1991) 427.

[26] H.Y. Choi, W.E. Slye, R.J. Fruehan, R.C. Nunnington, Metallurgical and Materials Transactions B 36b (2005) 537.

[27] S.A. Firstov, S.V. Tkachenko, N.N. Kuz'menko, Metal Science and Heat Treatment 51 (2009) 12.

[28] F. Unkić, A. Preloščan, V. Đukić, Materiali in Tehnologije 37 (2003) 19.

[29] S.C. Tjong, ISIJ International 31 (1991) 738.

[30] H.C. Brookes, J.W. Bayles, F.J. Graham, Journal of Applied Electrochemistry 20 (1990) 223.

[31] M.H. Ras, P.C. Pistorius, Corrosion Science 44 (2002) 2479.

[32] D. Chaliampalias, G. Vourlias, E. Pavlidou, G. Stergioudis, K. Chrissafis, Applied Surface Science 255 (2009) 6244.

[33] J. Michel', M. Buršák, M. Vojtko, Materials Engineering 18 (2011) 57.

[34] F.A. Garner, H.R. Brager, D.S. Gelles, J.M. McCarthy, Journal of Nuclear Materials 148 (1987) 294.

[35] S.C. Tjong, Applied Surface Science 45 (1990) 141.

[36] P. Hohenberg, W. Kohn, Phys. Rev. 136 (1964) B864.

[37] W. Kohn, L.J. Sham, Phys. Rev. 140 (1965) A1133.

[38] L. Vitos, Computational Quantum Mechanics for Materials Engineers: The EMTO Method and Applications, Engineering Materials and Processes Series, London, Springer-Verlag (2007).

[39] L. Vitos, I.A. Abrikosov, B. Johansson, Phys. Rev. Lett. 87 (2001) 156401.

[40] O.K. Andersen, O. Jepsen, G. Krier, Lectures on Methods of Electronic Structure Calculations, ed. V. Kumar, O.K. Andersen, A. Mookerjee, Singapore, World Scientific Publishing Co. (1994) p. 63–124.

[41] O.K. Andersen, C. Arcangeli, R.W. Tank, T. Saha-Dasgupta, G. Krier, O. Jepsen, I. Dasgupta, Tight-Binding Approach to Computational Materials Science, ed. P.E.A. Turchi, A. Gonis, L. Colombo, Materials Reseach Society, Pittsburg, Mater. Res. Soc. Symp. Proc. 491 (1998) 3.

[42] L. Vitos, Phys. Rev B 64 (2001) 014107.

[43] L. Vitos, H.L. Skriver, B. Johansson, J. Kollár, Computational Materials Science 18 (2000) 24.

[44] J.P. Perdew, K. Burke, M. Ernzerhof, Phys. Rev. Lett. 77 (1996) 3865.

[45] P. Olsson, I.A. Abrikosov, J. Wallenius, Phys. Rev. B 73 (2006) 104416.

[46] P. Olsson, I.A. Abrikosov, L. Vitos, J. Wallenius, Journal of Nuclear Materials 321 (2003) 84.

[47] P. Soven, Phys. Rev. 156 (1967) 809.

[48] B.L. Györffy, Phys. Rev. B 5 (1972) 2382.

[49] G.J. Ackland, Phys. Rev. Lett. 97 (2006) 015502.

[50] M. Ropo, K. Kokko, M.P.J. Punkkinen, S. Hogmark, J. Kollár, B. Johansson, L. Vitos, Proceedings of 6$^{\text{th}}$ European Stainless Steel Conference, Science and Market, Helsinki, Finland, June 10–13, 2008, ed. P. Karjalainen and S. Hertzman (Jernkontoret) (2008) pp. 323–326.

[51] M. Ropo, K. Kokko, E. Airiskallio, M.P.J. Punkkinen, S. Hogmark, J. Kollár, B. Johansson, L. Vitos , J. Phys.: Condens. Matter 23 (2011) 265004.

[52] P. Olsson, C. Domain, J. Wallenius, Phys. Rev. B 75 (2007) 014110.

[53] T.P.C. Klaver, R. Drautz, M.W. Finnis, Phys. Rev. B 74 (2006) 094435.

[54] A. Kiejna, E. Wachowicz, Phys. Rev. B 78 (2008) 113403.

[55] A.V. Ruban, P.A. Korzhavyi, B. Johansson, Phys. Rev. B 77 (2008) 094436.

[56] H.C. Herper, E. Hoffmann, P. Entel, J. Mag. Mag. Mater. 240 (2002) 401.

[57] H.C. Herper, E. Hoffmann, P. Entel, Phase Transit. 75 (2002) 185.

[58] B. Nonas, K. Wildberger, R. Zeller, P.H. Dederichs, Phys. Rev. Lett. 80 (1998) 4574.

[59] E. Airiskallio, E. Nurmi, I.J. Väyrynen, K. Kokko, M. Ropo, M.P.J. Punkkinen, B. Johansson, L. Vitos, Phys. Rev. B 80 (2009) 153403.

[60] E. Airiskallio, E. Nurmi, M.H. Heinonen, I.J. Väyrynen, K. Kokko, M. Ropo, M.P.J. Punkkinen, H. Pitkänen, M. Alatalo, J. Kollár, B. Johansson, L. Vitos, Corrosion Science 52 (2010) 3394.

[61] L. Vitos, A.V. Ruban, H.L. Skriver, J. Kollár, Surface Science 411 (1998) 186.

[62] M. Ropo, K. Kokko, L. Vitos, J. Kollár, B. Johansson, Surface Science 600 (2006) 904.

[63] A.E. Kissavos, S.I. Simak, P. Olsson, L. Vitos, I.A. Abrikosov, Computational Materials Science 35 (2006) 1.

[64] G.J. Ackland, Phys. Rev. B 79 (2009) 094202.